Entrances, Traps, and Rate-controlling Factors for Nickel-Catalyzed C-H Functionalization

Alex J. Nett, John Montgomery,* and Paul M. Zimmerman*

Department of Chemistry, University of Michigan, 930 North University Avenue, Ann Arbor, Michigan 48109-1055, United States

ABSTRACT: A detailed mechanistic investigation of N-heterocyclic carbene-nickel-catalyzed hydroarylation via C-H functionalization is described. These catalysts are complicated, in part, by undesired reactivity stemming from common olefinic ligands such as cyclooctadiene (COD) that stabilize the pre-catalyst. This reaction adds diversity to the overall reactive landscape by permitting multiple types of ligand-to-ligand hydrogen transfer (LLHT) steps to activate the substrate arene C-H bonds. In one case, stable π-allyl complexes can be formed via LLHT to the olefin, hindering catalysis, and in the other, LLHT to the alkyne substrate leads to productive catalysis. Here, a useful map is built from extensive computational and experimental studies to guide subsequent investigations on the productive use of Ni catalysis. In addition to showing the details of catalyst deactivation, activation, and operating regimes, this article suggests that: 1. Reductive elimination is rate-limiting and assisted by an additional alkyne ligand, 2. The resting state for catalysis is an alkyne-ligated Ni center, and 3. the reaction rate is under thermodynamic control, showing a good correlation with thermodynamics of C-H addition to the metal center ($R^2 = 0.95$).

KEYWORDS: nickel catalysis, C-H functionalization, chain walking, off-cycle activity, linear free energy relationships

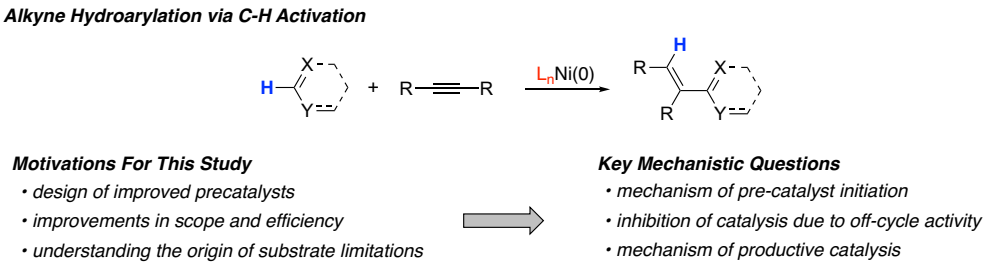

Figure 1. Motivations for investigating nickel-catalyzed hydroarylations.

Introduction

Carbon-hydrogen bond functionalization has emerged as an atom-economical route to many interesting chemical scaffolds.[1] Although the bulk of these methods utilize second and third row transition metals, recent developments have enabled many unique and promising transformations that employ base metals as catalysts.[2] Our specific interests are in the unique capabilities and mechanistic features of nickel-based C-H functionalization catalysis. Inspired by the pioneering work from Hiyama and Nakao demonstrating the utility of nickel-catalyzed hydroarylation of alkynes,[3] our efforts have focused on the mechanistic details of this reaction class and the identification of rationally designed catalysts that demonstrate improved scope and activity.[4] Although many valuable synthetic schemes have been reported in this area, these strategies are limited by high catalyst loadings, elevated temperatures, narrow substrate scope, and the presence off-cycle pathways that inhibit catalyst efficiency. In-depth mechanistic information is clearly needed to fully exploit these catalytic processes and to accelerate catalyst design for new transformations (Figure 1).

To this end, nickel-mediated C-H activation has been shown to operate through base-assisted C-H bond cleavage,[5] or ligand-to-ligand hydrogen transfer (LLHT), where the oxidative addition of a C-H bond occurs in concert with migratory insertion of an unsaturated co-reactant.[6] C-H activation during nickel-catalyzed hydroarylation is proposed to be reversible[7] and generally thought to proceed through LLHT as the primary mode for C-H activation.[7d,8] A seminal computational mechanistic study by Perutz describing phosphine-nickel mediated LLHT during alkyne hydroarylation showed reactions are more sensitive to Ni-C bond strength than the lability of the C-H bond.[6] We sought to explore this area further by developing a comprehensive model that is supported by extensive simulations and experimental findings.

Recently, it has been observed that common olefinic ligands used to stabilize nickel pre-catalysts can interrupt catalysis, rather than allowing the catalyst to form product.[4,9] Specifically, it was found that cyclooctadiene (COD) promotes LLHT and leads to COD-derived π-allyl complexes that inhibit catalysis. Other examples of non-innocent COD-based reactivity have been described previously in the literature.[10] Since most nickel-catalyzed methods developed for organic synthesis utilize bis(cyclooctadiene) nickel (0) ($Ni(COD)_2$) as a pre-catalyst, this type of activity becomes highly relevant.[11] Although there have been several contributions that describe isolated mechanistic features of the reactive landscape for this class of reactions, a working model that links pre-catalyst initiation to on- and off-cycle reaction pathways, as well as provides experimental evidence for the physical properties governing reactivity, is needed (Figure 1).

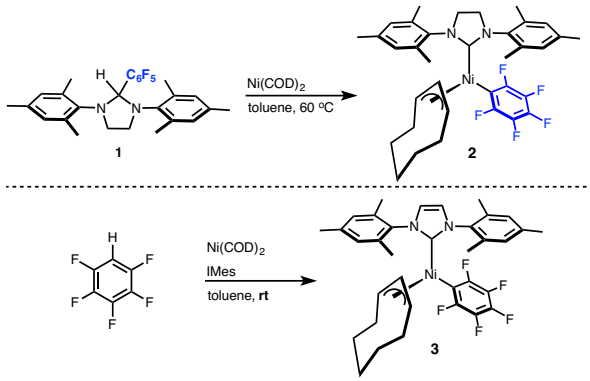

Figure 2. Two routes for the formation of π-allyl complexes.

The fate of COD in nickel-catalyzed C-H functionalization was initially realized when exploring the use of pentafluoroaryl-NHC precursors (**1**).[12] It was observed that thermolysis of **1**, generating SIMes and free C_6F_5H, in the presence of $Ni(COD)_2$ led to direct capture of the C-H bond in C_6F_5H via LLHT to COD, ultimately leading to π-allyl complex **2** (Figure 2). Alternatively, an analogous π-allyl complex, **3**, with IMes could be readily synthesized at room temperature in the presence of $Ni(COD)_2$ and C_6F_5H.

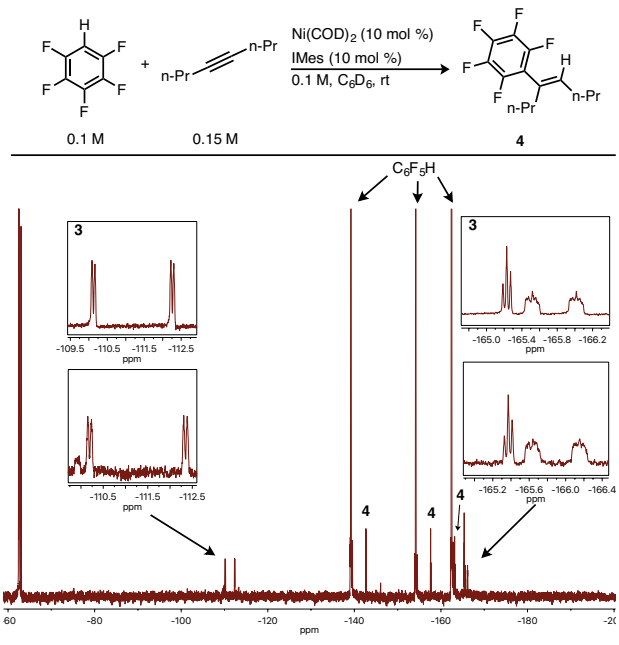

Figure 3. Reaction monitored by ^{19}F NMR which shows the presence of **3** in a productive reaction. The full spectrum and lower inlays are of the catalytic reaction. The upper inlays are of independently synthesized complex **3**.

Given the widespread employment of $Ni(COD)_2$ as a pre-catalyst, these observations brought into question the role that complexes analogous to **2** and **3** play during nickel-catalyzed arene C-H bond functionalization. Our initial efforts in characterizing the impact of **3** during catalysis demonstrated that **3** forms in low concentrations during nickel-catalyzed hydroarylation reactions (Figure 3). Furthermore, it was also shown that the formation of **3** is highly exergonic and its formation drastically inhibits catalysis. The experimental and computational data suggested that **1** acts as an off-cycle thermodynamic sink that impedes productive catalysis. Motivated by this result we searched for alternative COD-free pre-catalysts. The discrete 1,5-hexadiene-stabilized NHC-Ni pre-catalyst (**5**, Figure 4) was identified as an excellent alternative to COD, as off-cycle activity is avoided, leading to highly efficient catalysis at room temperature. While the synthetic consequences of pre-catalyst choice and effects of off-cycle activity were discussed in our previous report,[4] the sensitivity of ligand substitution/pre-catalyst initiation were only qualitatively described and complete mechanisms for π-allyl formation and active catalysis were not disclosed.

Reported herein is a mechanistic study describing a wide spectrum of the reaction mechanisms governing catalyst initiation, off-cycle activity, and on-cycle catalysis. The computed energetic map of the landscape is corroborated with experimental kinetic analysis to identify a potential resting state for nickel-catalyzed hydroarylations. Additionally, two competing mechanisms for the formation of off-cycle π-allyl intermediates are proposed, involving either classical nickel-mediated chain-walking via nickel hydrides or iterative LLHT. Ultimately, a mechanism for product-forming nickel-catalyzed hydroarylation is developed, and analysis of the rates and energetics for a broad range of substrates shows that nickel-mediated C-H activation can be operative under thermodynamic control in specific catalytic conditions.

Results and Discussion

Pre-Catalyst Initiation

To fully understand the relationship between choice of pre-catalyst and entry into either productive catalysis or off-cycle π-allyl formation, we began assessing hydroarylation pathways starting from either IMes-Ni-COD, **6**, or the analogous 1,5-hexadiene stabilized pre-catalyst, **5**. The model system was chosen to be the coupling of 4-octyne and C_6F_5H, and various intermediates that form via ligand substitution en route to the active catalyst were investigated (Figure 4). The binding energy of 1,5-hexadiene to the Ni center in **5** is 15.6 kcal/mol more stable than **6**, which explains why **5** is isolable, but **6** must be made *in situ*. From these two precatalysts, Figure 4 shows the thermodynamic landscape leading to the most plausible intermediates of active catalysis.

From **6**, pentafluorobenzene addition to form complex **7a** is endergonic by 8.0 kcal/mol, whereas the coordination of 4-octyne is exergonic by 6.6 kcal/mol (**8a**). In each case, one of the Ni-π bonds is displaced to produce 3-coordinate Ni complexes. The preference for octyne over pentafluorobenzene is likely due to increased back-bonding by alkynyl ligands compared to η^2-arene π-coordination. From precatalyst **5**, coordination of either substrate is endergonic due to the higher stability of the 1,5-hexadiene complex. This endergonicity holds for full dissociation of the diene ligand from **7** or **8** to yield 2-coordinate complexes with pentafluorobenzene (**10**) or 4-octyne (**9**). Coordination of an additional 4-octyne to **9** forms three-coordinate complex **11**, which is exergonic by 5.3 kcal/mol from **9**. Likewise, coordination of 4-octyne to **10** leads to complex **12**, which is the first species taking part in productive catalysis. Although complex **12** with an arene and an alkyne is needed for catalysis, the bis-alkyne intermediate **11** is 8.3 kcal/mol more stable (Figure 4).

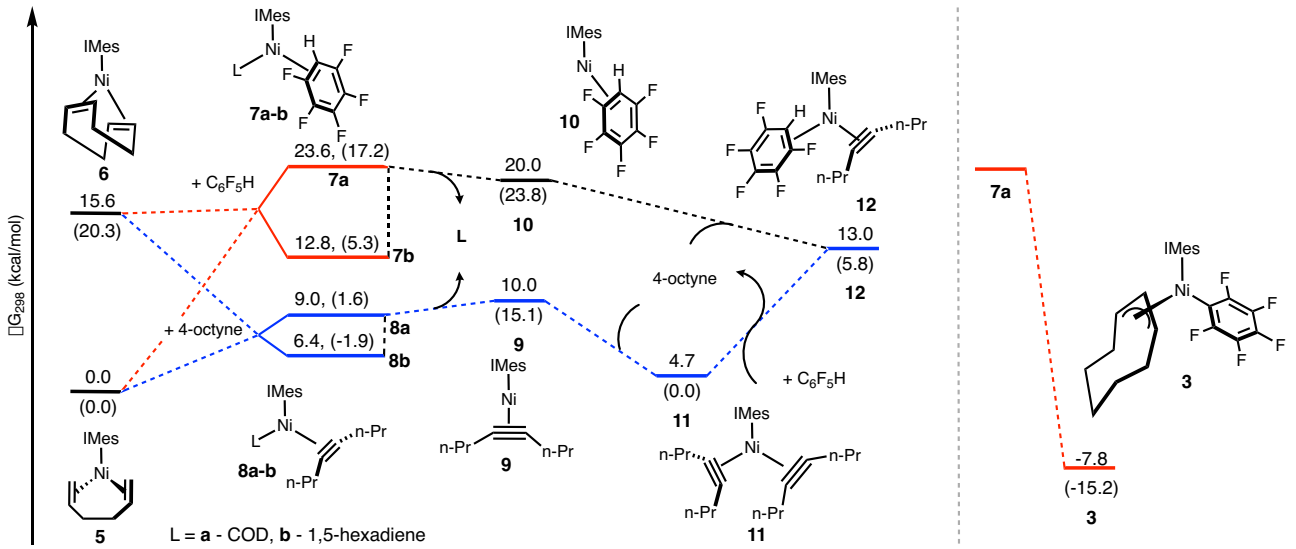

Figure 4. Thermodynamic map of intermediates preceding catalysis. All free energies (ωB97X-D/cc-pVTZ/SMD) in kcal/mol. Enthalpies are shown in parenthesis in kcal/mol. Red: leads to off-cycle pathways. Blue: leads to product forming catalysis.

Overall, the computational analysis suggests that regardless of pre-catalyst choice, the most thermodynamically favorable ligand substitution proceeds with 4-octyne, through intermediate **9**. Attachment of another 4-octyne is thermodynamically favorable and leads to complex **11** where the nickel center is coordinated to two alkyne ligands (blue, Figure 4). Precatalyst initiation thus requires alkyne as the first substrate.

Ancillary Ligand Activity

The productive pathways from precatalyst to the active catalytic intermediates can be interrupted by COD-promoted C-H activation via LLHT (Figure 3).[4] From **6**, this reaction consumes the aryl substrate and leads to the π-allyl, **3**, which was previously proposed to form through a series of chain walking events. The mechanism of this sequence has not yet been described.[13] Although the use of transition metal-mediated chain walking, more specifically nickel, has shown great synthetic value,[14] there is limited information available for β-agostic interactions with neutral nickel complexes.[15,16] Therefore, the pathways to **3** from **7a** were investigated in detail.

Starting from complex **7a**, cleavage of the C-H bond in pentafluorobenzene proceeds through LLHT to a COD olefin (Figure 5). This process has a relatively low barrier of 5.5 kcal/mol (**TS-7a-13**) and is exergonic by -11.5 kcal/mol (**13**). Intermediate **13** has a strong β-agostic interaction with the newly formed C-H bond and consequentially is slightly elongated (Figure 5). While this activation opens the possibility for β-hydrogen elimination and reinsertion to walk around the ring, we also found a second mechanism could be operative. The second case involves reversing the LLHT C-H activation at a unique COD hydrogen, permuting the ring's attachment point to nickel.

These two possible mechanisms were studied, the first involving traditional chain walking, and the second involving nontraditional H-transfer directly to the C-H activated ligand. Both mechanisms begin at agostic complex **13**, where rotation of the Ni-C_{COD} bond (via **TS-13-14**) transfers the agostic interaction towards a productive alignment for π-allyl formation (Figure 5). At this point (**14**) the two mechanisms for π-allyl formation diverge, where traditional chain walking through β-hydride elimination results in a nickel-hydride complex (**15a**), or alternatively LLHT reforms the C-H bond in pentafluorobenzene (**15b**, Figure 6).

For traditional chain walking, β-hydride elimination forms an unstable and short-lived square planar nickel hydride complex **15a**, where the hydride is *trans* to the carbene. The endergonic nature of **15a** is consistent with β-agostic C-H bonds to nickel generally being stronger than the analogous Ni-H bonds.[7] Through a nearly barrierless transformation (**TS-15a-16**), the newly formed olefin in **15a** inserts into the nickel-hydride to give agostic complex **16,** where the ring is one

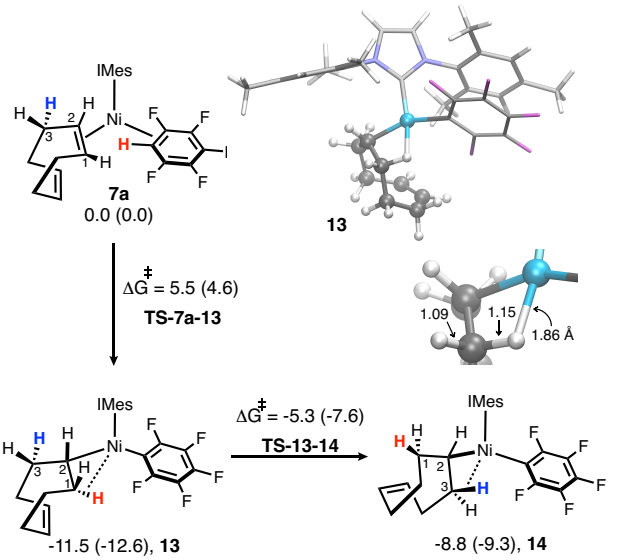

Figure 5. Agostic transfer from Ni-H-C1 to Ni-H-C3. All free energies (/ωB97X-D/cc-pVTZ/SMD) in kcal/mol, with enthlapies in parenthesis.

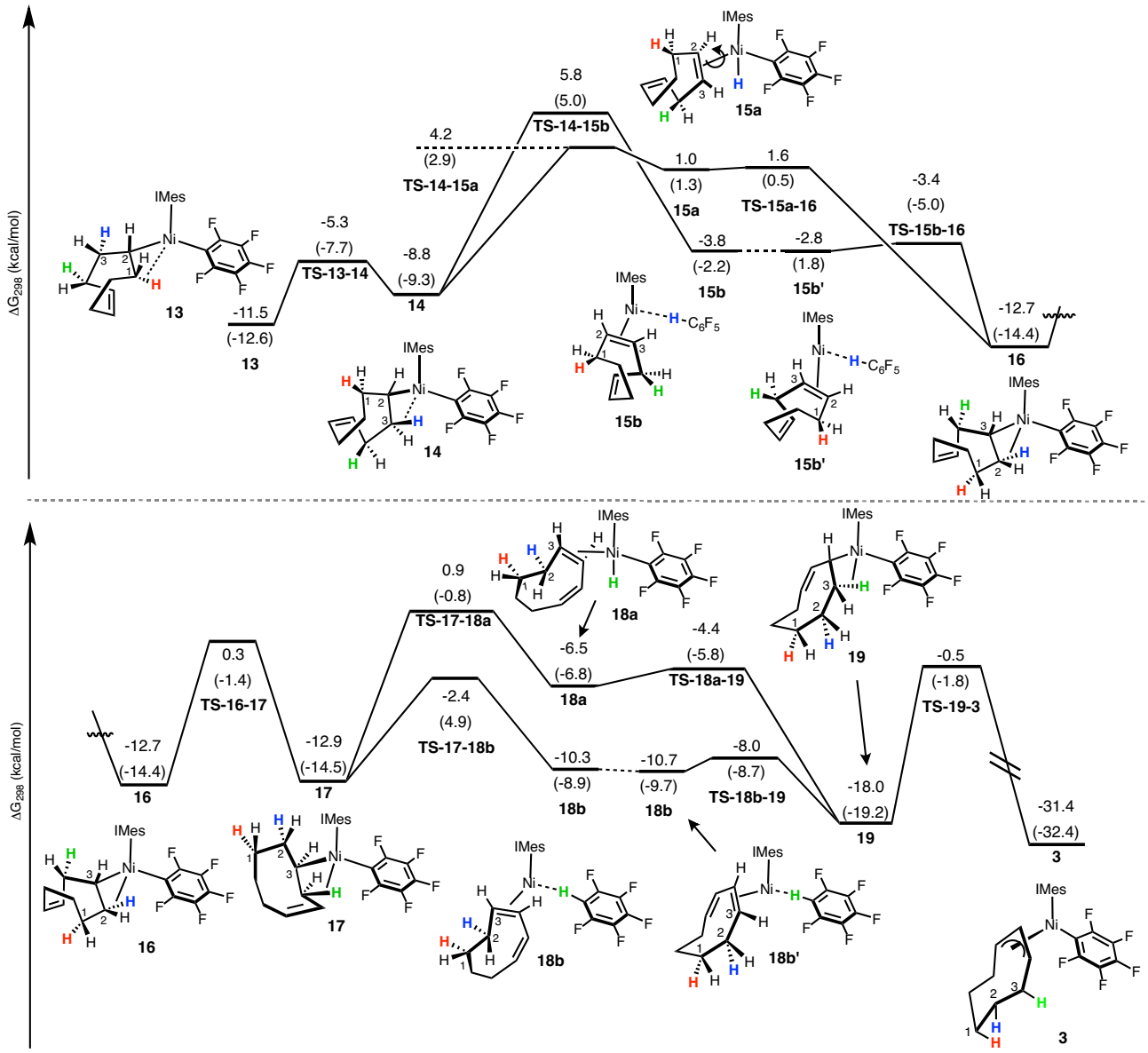

Figure 6. Complete mechanism for chain walking via iterative nickel-hydride formation and LLHT. All free energies (ωB97X-D/cc-pVTZ/SMD) in kcal/mol, with enthalpies in parenthesis.

carbon closer to the second olefin. In analogous steps to the **13-14-15a-16** sequence, the pathway through **16-17-18a-19** walks the ring to position the C-Ni bond proximal to the olefin. From **19**, transfer of the σ-allyl-Ni interaction to π-allyl coordination results in complex **3**, which is exergonic by 31.4 kcal/mol from **7a** (Figure 6).

Alternatively, hydrogen transfer (LLHT) to the pentafluorobenzene ligand in **14** allows chain walking without the formation of any discreet Ni hydride intermediates. The 5.8 kcal/mol barrier for LLHT from C3 to pentafluorobenzene (**TS-14-15b**, Figure 6) is consistent with the reverse of the C-H activation LLHT step forming **7a** from **13** (Figure 5). By placing the H on pentafluorobenzene, rather than on Ni, the barrier for a single chain-walking step is similar to traditional chain walking, but the resulting intermediate (**15b**) is much more stable, at 4.8 kcal/mol below **15a**. LLHT from pentafluorobenzene back to 1,4-cyclooctadiene results in complex **16**, which marks the completion of a single chain walking step.

Repeating the LLHT swapping process ultimately leads to the formation of **3**, as shown in Figure 6. The early steps to the formation of **3** show that chain-walking via transient nickel-hydrides or iterative LLHT are energetically similar. Later in the pathway, there is an energetic preference to proceed through reversible LLHT as a means of olefin migration. Nevertheless, both pathways are kinetically feasible at room temperature and likely compete to reach formation of **3**.

With the facile chain-walking pathways leading to the π-allyl complexes in mind, we now turn to the full thermodynamic map of Figure 4 to discuss strategies for avoiding this pathway. From **6**, the addition of pentafluorobenzene leads to **7a**, the precursor for **3**. This ligand substitution is uphill in free energy by 8 kcal/mol. Alternatively, the addition of 4-octyne to **6** instead of pentafluorobenzene forms complex **8a**, and a second addition of 4-octyne fully displaces COD and gives **11**, which is 10.9 kcal/mol downhill from **6**. This landscape suggests that the equilibrium between **11** and **7a** could play an

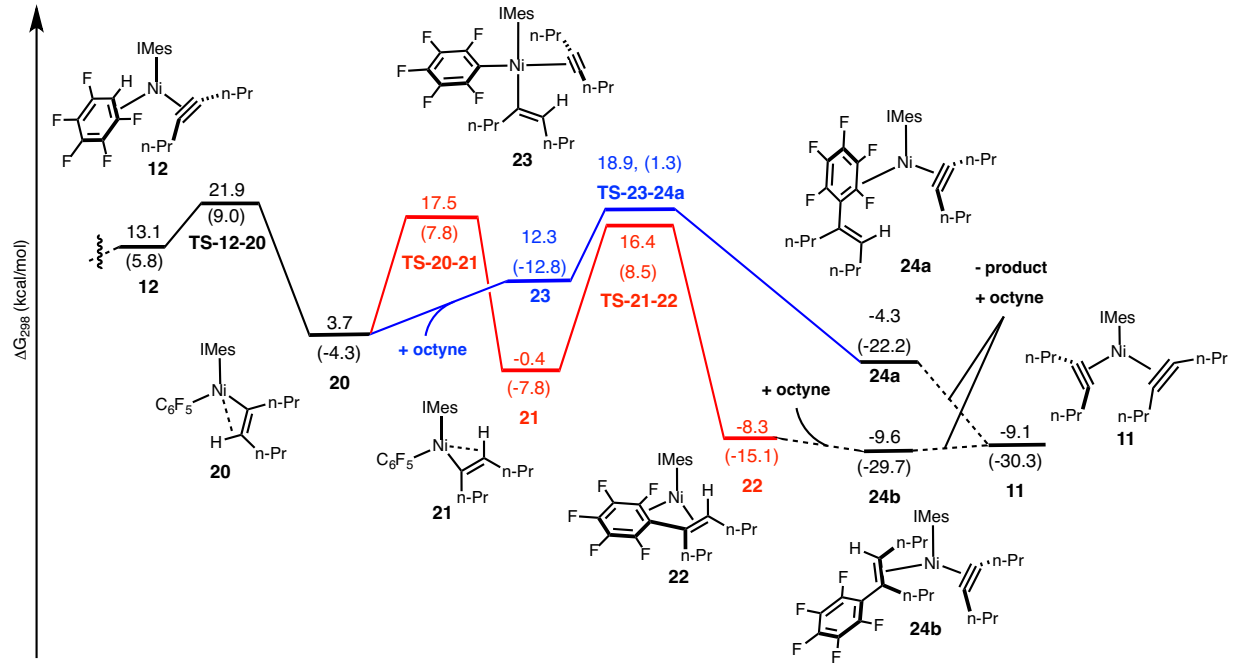

Figure 7. Mechanism for Ni-IMes catalyzed hydroarylation of alkynes, referenced to **4**, Figure 2. All free energies (ωB97X-D/cc-pVTZ/SMD) in kcal/mol, with enthalpies in parenthesis. Red - three-coordinate reductive elimination pathway. Blue - four-coordinate reductive elimination pathway.

important role in regulating catalytic activity, as **11** moves the catalyst towards product formation, and **7a** towards the π-allyl trap, **3**. The relative amounts of **11** and **7a** in the reaction media could likely be modified by reordering the substrate addition sequence. This is especially important since it is commonplace to add alkyne reagents last to minimize nickel-catalyzed alkyne trimerization.[3c]

To probe the effects of addition order, the coupling of pentafluorobenzene and 4-octyne catalyzed by $Ni(COD)_2$/IMes was monitored by ^{19}F NMR. In our original protocol, arene was first added to the catalyst solution, followed immediately by addition of alkyne. In that case, the reaction was slow at room temperature, forming only a trace amount of product after one hour. When adding the two substrates as a single solution, a rapid burst of product is observed along with the formation of complex **3**. At the earliest time point (32 sec) the yield was 11 % and only reached 14 % yield after 30 minutes, suggesting that simultaneous addition of substrates allows formation of small amounts of product and **3**. Interestingly, when 0.5 eq. 4-octyne is added prior to the addition of 1.0 eq. pentafluorobenzene and 1.0 eq. 4-octyne, a much more efficient reaction is produced (see Supporting Information).

The benefits of early addition of alkyne is consistent with equilibration between ligation of COD and alkyne prior to catalysis. Once arene is added to the reaction mixture, COD-ligated species (**7a**) rapidly leads to π-allyl complexes (**3**) and alkyne ligated nickel (**9** and **11**) goes on to form the coupling product (Figure 4). The order of addition experiments also suggest that the formation of **3** is irreversible at room temperature and that productive catalysis is regulated by the amount of alkyne-ligated species (**9** and **11,** Figure 4). Nevertheless, optimal reactivity is reached by utilizing pre-catalysts like **5** which do not contain COD or promote off-cycle activity.

Hydroarylation Mechanism

Computational Analysis

Having established the mechanistic aspects of off-cycle activity, the mechanism for product-forming catalysis was investigated. Starting from **5** as the optimal pre-catalyst for hydroarylation, catalysis conceptually begins with intermediate **12**, where the NHC-Ni is ligated by 4-octyne and pentafluorobenzene (LLHT to 1,5-hexadiene was previously shown to be implausible due to its high activation barrier).[4] From **12**, C-H activation proceeds through LLHT from pentafluorobenzene to 4-octyne (**TS-12-20**, Figure 7) with a barrier of 8.8 kcal/mol. This pathway is relatively low barrier because it leads directly to stable β-agostic complex **20**, which is 9.4 kcal/mol downhill from **12** (Figure 7), and avoids high energy Ni-hydride intermediates. C-H activation was previously demonstrated to be reversible for related systems[7,8] and this is consistent with the reverse reaction (**20** to **12**, with an 18.2 kcal/mol barrier) being kinetically feasible. To achieve C-C bond forming reductive elimination from **20**, cleavage of the β-agostic interaction and rotation of the nickel-vinyl bond is required. Rotation of the nickel-vinyl bond to form complex **21** has a 13.8 kcal/mol barrier through **TS-20-21**. From **21**, reductive elimination via **TS-21-22** has a barrier of 18 kcal/mol to form **23**, which has bidentate coordination of the product to the nickel center, and is exergonic by 7.9 kcal/mol from **21**. Alternatively, reductive elimination could be assisted by coordination of an additional equivalent of 4-octyne to form four coordinate complex **23**. Although complex **23** is higher in energy than **21** by 12.7 kcal/mol, reductive elimination from **23** proceeds through **TS-23-24a** and requires 18.9 kcal/mol which is only 2.5 kcal/mol above **TS-21-22** (Figure 7). Reductive elimination from **23** results in the formation of three-coordinate complex **24a**, 16.6 kcal/mol downhill from **23**. The free energy for reductive elimination from **23** is in part

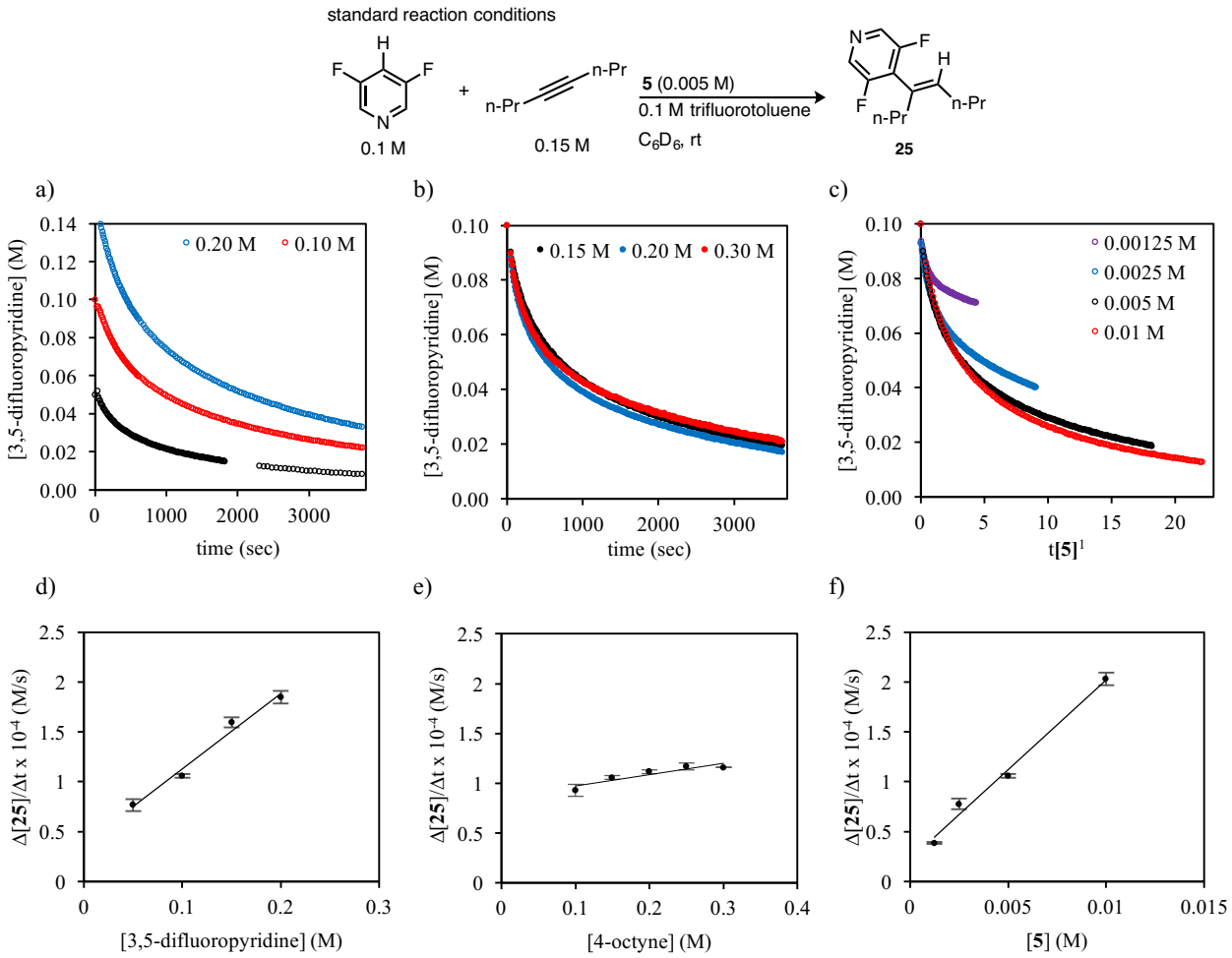

Figure 8. Plots of the initial rate of consumption of starting material. a.) Different excess experiment varying the concentration of 4-octyne. b). Different excess varying the concentration of 3,5-difluoropyridine. c.) Different excess varying the concentration of catalyst. Initial rate points are an average of three runs as a function of 3,5-difluorpyridine (d), 4-octyne (e), and **4** (f).

due to negative entropy of association, where the enthalpic requirement for **TS-23-24a** is 7.2 kcal/mol lower than **TS-21-22**. With an excess of 4-octyne in the reaction mixture, **23** will be further populated, and **TS-23-24a** will be more prevalent.

To complete the catalytic cycle, **22** or **24a** returns to an active catalytic species via substitution of the newly formed styrenyl product with 4-octyne. This mechanism proceeds via **22** by addition of 4-octyne, giving **24b**, 1.3 kcal/mol downhill from **22** (Figure 7). Next, complete dissociation of the styrenyl product from **24** by coordination of an additional equivalent of 4-octyne reforms **11**.

The data shown in Figure 7 suggest that either reductive elimination from a three-coordinate (**TS-20-21**) or a four-coordinate (**TS-23-24a**) intermediate is rate limiting. This assignment contrasts to a related study using phosphines, where rotation of the nickel-vinyl bond prior to reductive elimination was proposed to be rate-limiting.[6] The net-change in free energy for the transformation is -13.8 kcal/mol (Figure 4 and 7).

Experimental Kinetics

Since the two pathways for reductive elimination (Figure 7) are similar in energy, we next investigated the reaction profile using experimental kinetic analysis to provide further insights into the complete mechanism. Specifically, NMR was used to continuously monitor the progress of the reaction, generating profiles shown in Figure 8a-c. Although the computations described above (Figure 4 and 7) used pentafluorobenzene as the arene substrate, the rapid rate of reaction made it

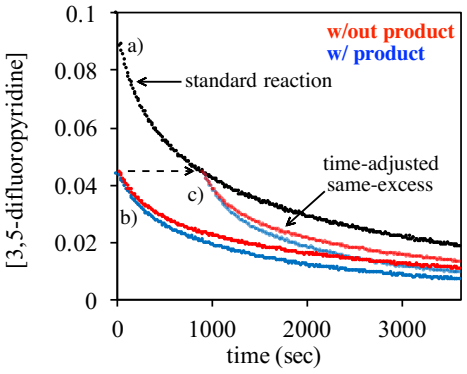

Figure 9. Concentration of 3,5-difluoropyridine as a function of time. (a) - standard reaction plot. (b) "same-excess" experiment. (c) - time adjusted "same-excess" experiment. Experiments were monitored by ^{19}F NMR, details and raw data can be found in the Supporting Information.

Table 1. Initial rate and energetic parameters for LLHT.

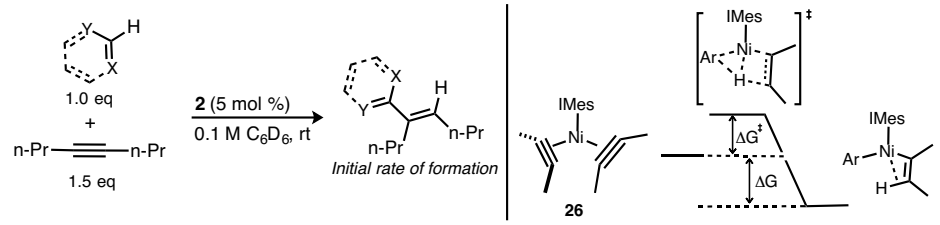

entry	substrate	initial rate (M/s)	ΔG (kcal/mol)[a]	ΔG‡ (kcal/mol)[a]
1	benzoxazole	--[d]	-7.8	12.7
2[c]	pentafluorobenzene	7.30 x 10^{-4}	-6.8	12.5
3[c]	1,2,4,5-tetrafluorobenzene	3.62 x 10^{-4}	-6.6	8.8
4[c]	3,5-difluoropyridine	1.10 x 10^{-4}	-4.7	14.6
5[b]	1,3-dimethyluracil	4.89 x 10^{-5}	-3.2	22.5
6[b]	4,5-dimethylthiazole	2.54 x 10^{-5}	-3.1	11.0
7[b]	benzofuran	2.60 x 10^{-5}	-2.7	12.4
8[c]	1,2,3,4-tetrafluorobenzene	3.70 x 10^{-6}	-0.7	12.3
9[b]	benzothiophene	1.71 x 10^{-7}	0.8	11.9
10	fluorobenzene	--	5.6	20.8

[a]All free energies (ωB97X-D/cc-pVTZ/SMD) in kcal/mol. [b,c]Initial rates were obtained from either ^{1}H[b] or ^{19}F[c] NMR. [d]Reaction rate too high for analysis.

challenging to obtain reliable rate data. Therefore, kinetic analysis was instead performed for the coupling of 3,5-difluoropyridine, a less activated arene, and 4-octyne (Figure 8).

The reaction order was determined by varying the initial concentration of each of the reaction components, then analyzing initial rates and the subsequent reaction progress.

Protocols from Reaction Progress Kinetic Analysis (RPKA), including "different-excess" and "same-excess," were also used to identify the concentration dependencies on the rate of the reaction and catalyst stability, respectively.[17] In these experiments, "different excess" refers to varying the difference in initial concentration of alkyne and arene. "Same excess" experiments adjust the initial concentrations of substrates while maintaining the same absolute difference in initial concentration of alkyne and arene. The significance of "same excess" is that these conditions represent the same reaction started from different points. The initial conditions are calculated such that the initial substrate concentrations for one reaction equals those of a second same excess reaction when it reaches a chosen conversion level, e.g., 25-50%. From that conversion onward, these two reactions should exhibit identical rates since they exhibit identical substrate concentration. "Overlay" between the two kinetic profiles indicates that the catalyst is robust, while a difference in rates between the two reactions implicates either catalyst deactivation or product inhibition.[17,18]

The standard reaction initial concentrations (black lines in Figure 8a-c) are as follows: 3,5-difluoropyridine (0.1 M), 4-octyne (0.15 M) and precatalyst **2** (0.005 M). Varying the concentration of 3,5-difluoropyridine shows a first-order rate dependence in arene substrate, suggesting that the arene is involved in the rate-limiting step of the reaction (Figure 8a and 8d). Varying the initial concentration of 4-octyne shows zero-order kinetics in alkyne (Figure 8b and 8e). The initial rate data shows there is a slight positive-order rate dependence at low concentrations, but as the concentration increases, the slope of the rate as a function of alkyne concentration approaches zero. Implications of the zero-order dependence in alkyne are discussed below.

Varying the initial concentration of **5** showed a first-order rate dependence in catalyst. Furthermore, we analyzed the full reaction profiles using a normalized time scale method. This method, reported by Burés, compares substrate concentration on a normalized time scale t[catalyst]^{n}, where *n* equals reaction order in catalyst.[19] Varying *n* until all reaction profiles at different concentrations overlay reveals the catalyst order. For all plots to overlay, the catalyst concentration must be constant over the course of the reaction. At low catalyst loadings (0.0025 and 0.00125 M, Figure 8c) the reaction plots do not overlay, however, suggesting that the catalyst concentration is not constant over time.

To further examine catalyst stability, "same excess" protocols were used to probe the degree of deactivation at later stages of the reaction (Figure 9). The initial concentrations of arene and alkyne for the "same excess" experiment 9(b) are the same as the standard reaction 9(a) at the time-point indicated. The resulting time-adjusted reaction 9(c) is much faster than 9(a), which suggests that the concentration of active catalyst in 9(a) is lower than in 9(c). This observation corroborates the result from the catalyst-order analysis (Figure 8c) that the catalyst is deactivating over time. The "same excess" experiment with added product illustrates that catalyst deactivation is not occurring due to product inhibition (Figure 9). Although there appears to be a slight rate enhancement of adding product at the beginning of the reaction, the difference is minor and could arise from styrenyl-product displacing 1,5-hexadiene on the pre-catalyst to form complexes analogous to **24b** (Figure 7). We speculate that trace impurities in the reaction mixture could be deactivating the catalyst. The high sensitivity of the active nickel-catalyst at low concentrations has been observed,[20] which is likely why relatively high catalyst loadings are needed for many nickel-catalyzed organic transformations.[11]

The results from the computational analysis and kinetics experiments corroborate several aspects of the reaction: (1) an alkyne-ligated intermediate, i.e. **11** (Figure 4), is proposed as

the resting state for catalysis, (2) there is a first-order rate dependence for catalyst and arene substrate, and (3) product inhibition is not occurring. Finally, computations predict that the rate-limiting step is reductive elimination from either a three- (**TS-21-22**) or four-coordinate complex (**TS-23-24a**). Since the proposed resting state for catalysis contains two alkyne ligands (**11**, Figure 4), ligand substitution with arene to form **12** would result in inverse first-order dependence in alkyne (Figure 4). Therefore, if the reaction is overall zero-order in alkyne, incorporation of alkyne in the rate-limiting step is likely. The kinetic data presented herein suggest that rate-limiting reductive elimination occurs from four-coordinate complex, **23**, which requires a second alkyne (**TS-23-24a**, Figure 7). Due to the typically high concentration of alkyne in the reaction, this assignment is plausible.[3,4]

Kinetic versus Thermodynamic Control

A common limitation in nickel-catalyzed C-H functionalization reactions is the restriction to relatively acidic C-H bonds. Since the success of employing both computation and experiment for determining the underlying principles that govern reactivity has been previously demonstrated,[21] we evaluated the relationship between free energies for nickel-mediated C-H bond cleavage and initial rates for the coupling of a variety of C-H bond substrates with 4-octyne.

Previous examples of this type of energetic analysis for C-H bond activation have focused on quantifying M-C bond dissociation energies (BDE), which are difficult to obtain, and identifying correlations with well-known C-H BDEs.[22] Few studies, however have evaluated correlations between the initial rate of C-H functionalization versus computed barriers and thermodynamic driving forces for C-H bond cleavage.

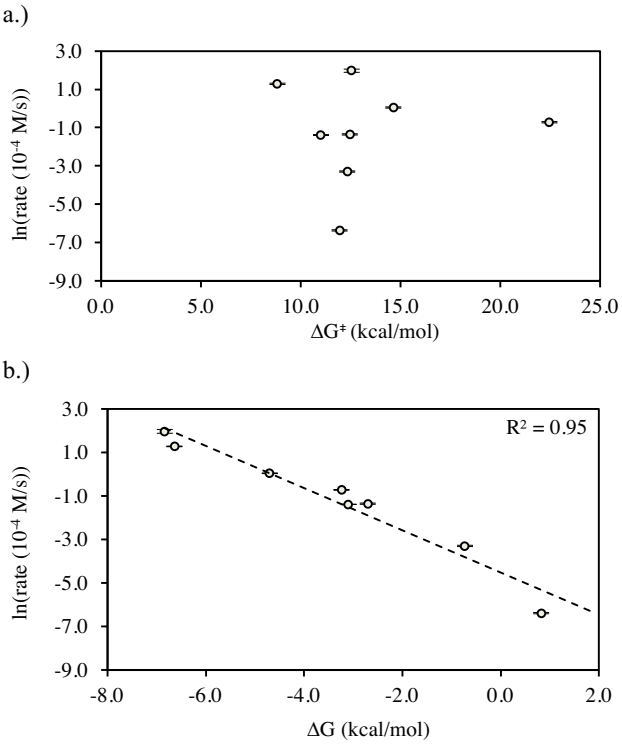

Figure 10. (a) Initial rate versus transition state energy for C-H bond cleavage. (b) initial rate versus thermodynamics for C-H bond cleavage.

Here, we consider the correlation between experimentally determined initial rates with reaction barriers ($\Delta G^{\ddagger}$) and thermodynamics (ΔG) of C-H bond cleavage and nickel-C_{aryl} bond formation (Table 1). Initial rates for **5**-catalyzed coupling of 4-octyne with each of the substrates in Table 1 were obtained using ^{1}H and ^{19}F NMR in C_6D_6. Due to limitations in the experimental setup, pentafluorobenzene was the fastest substrate where a reliable initial rate could be obtained, with an initial rate of 1.0×10^{-4} M s^{-1} (entry 2, Table 1). Conversely the slowest substrate tested was benzothiophene with an initial rate of 3.0×10^{-8} M s^{-1} (entry 9, Table 1).

The free energies for C-H activation ($\Delta G^{\ddagger}$) and Ni-C bond formation (ΔG) were obtained using density functional theory, with barriers being calculated using the growing string method[23] (Table 1, see Supporting Information for full details). Although the initial rates were obtained using 4-octyne, the LLHT step was calculated for each arene using 2-butyne as a model system. Energies for the transition state for C-H bond cleavage and the resulting nickel-aryl complex were referenced to a bis(butyne)-ligated nickel complex, **26** (Table 1).

The most facile C-H activation substrate, pentafluorobenzene, has a barrier of 12.5 kcal/mol (entry 2, Table 1), whereas 1,3-dimethyluracil has the highest barrier for C-H activation, 22.5 kcal/mol (entry 5, Table 1). Unsurprisingly, all the barriers calculated for C-H bond cleavage are surmountable at room temperature. The C-H bond insertion thermodynamics ranged from benzoxazole (entry 1, Table 1) being the most favorable, and fluorobenzene being the least favorable and endergonic (entry 11, Table 1).

When ΔG and $\Delta G^{\ddagger}$ for each of the substrates in Table 1 are plotted versus initial rate, ΔG correlates well, and $\Delta G^{\ddagger}$ does not (Figure 10). In Figure 10a, significant scatter exists between $\Delta G^{\ddagger}$ and the initial rate, indicating that C-H activation is not rate-controlling, consistent with our studies shown above. For example, benzofuran (entry 8, Table 1) and benzothiophene (entry 9, Table 1) have virtually the same barrier for C-H bond cleavage, yet the initial rate for benzofuran is two-orders of magnitude faster than benzothiophene.

On the other hand, comparing ΔG for benzofuran to benzothiophene shows that C-H activation is approximately 3 kcal/mol more thermodynamically favorable for benzofuran (entry 8, Table 1) than benzothiophene (entry 9, Table 1). The same sensitivity to ΔG is observed throughout the remaining substrates, and a linear free-energy relationship is observed with a correlation factor (R^2) of 0.95 (Figure 10b) for ΔG compared to ln(rate). To validate the hypothesis that thermodynamics of C-H activation correlates to reactivity, the energetics for fluorobenzene (entry 10, Table 1), a substrate that does not form product under the reaction conditions, show that the barrier for C-H activation was calculated to be 20.8 kcal/mol, but more importantly the C-H bond cleavage event is endergonic by 5.6 kcal/mol. According to the proposed thermodynamic control in this reaction, product formation is unfavorable, consistent with experiment.

Interestingly, this means that thermodynamically favored C-H activations are favored across several classes of substrates, which fully accounts for the chemoselectivity for nickel-catalyzed C-H functionalization. This is plausible considering that computations support reductive elimination (**TS-23-24a**, Figure 7) as the rate-limiting step of the reaction. Given this rate-limiting step, populating the C-H inserted intermediate prior to it controls the rate. Identifying ligand scaffolds that do

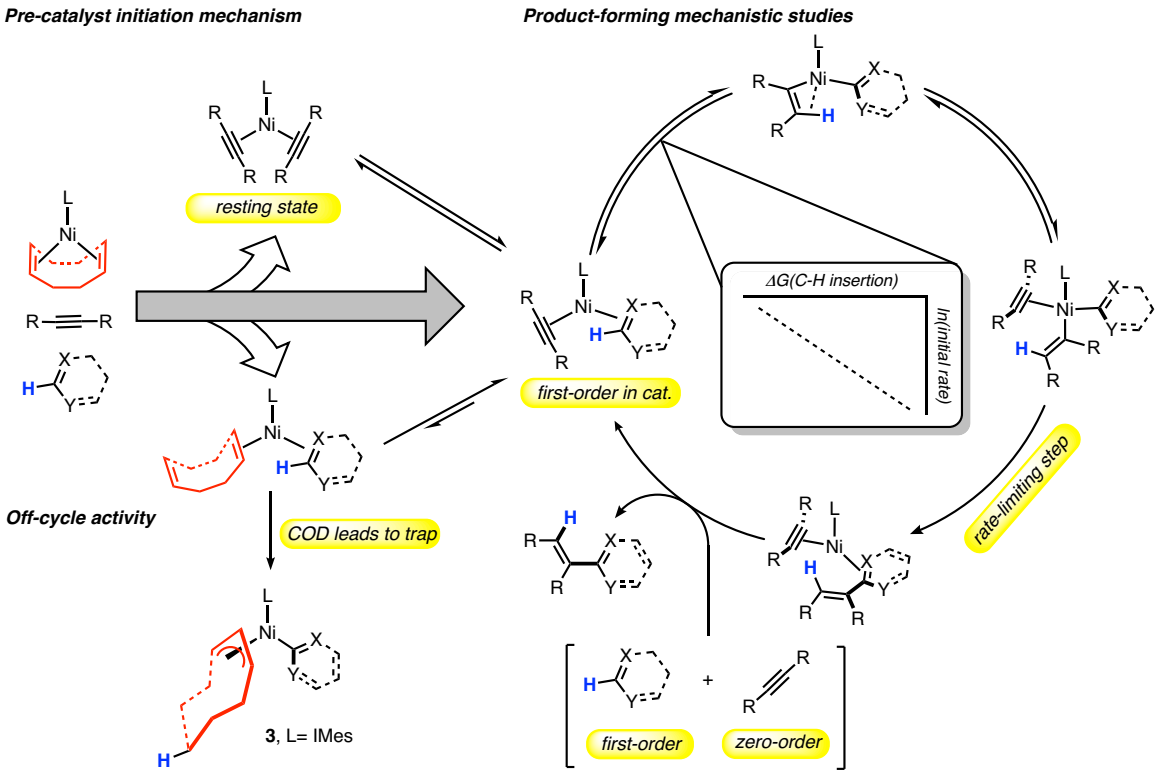

Figure 11. Overall map of catalyst deactivation, activation, and productive catalysis.

not follow this trend or ligands that promote thermodynamically favorable C-H bond activations for less activated C-H bonds, for example benzothiophene, could lead to either unique C-H bond selectivity or significant increases in reactivity.

Conclusion

Ligand substitution during pre-catalyst initiation and potential off-cycle inhibitory activity lead to considerable complexities in nickel-catalyzed C-H functionalizations. In support of this, there is potential for competing reactivity involving COD whenever $Ni(COD)_2$ is the pre-catalyst. Earlier reports from our group have shown that COD-mediated pathways ultimately result in the formation of π-allyl complexes (**3**, Figure 2), which significantly inhibit catalysis.[4] The current report shows that the formation of **3** (Figure 6) can proceed through either traditional chain walking via nickel-hydrides or through reversible LLHT events. Complementary to these studies, experiments show π-allyl complexes form during hydroarylation catalysis regardless of order of substrate addition. To avoid off-cycle π-allyl forming activity it is necessary to adapt the catalytic system to remove COD. Our efforts have focused on employing **5** which utilizes 1,5-hexadiene as a stabilizing ligand on the nickel pre-catalyst which does not promote LLHT at room temperature.

Kinetic and computational analysis of nickel-catalyzed hydroarylations via C-H functionalization reveal that the reactions is overall second-order, being first-order in arene and catalyst. Zero-order kinetics in alkyne agree with the simulation results that suggest the resting state for catalysis is a bis-alkyne ligated nickel species (**11**, Figure 7). Computation and kinetic data also suggests that the rate limiting step is reductive elimination (**TS-23-24a**, Figure 7). These results are corroborated by correlations between experimentally measured initial rates and computed energetic parameters. Specifically, the results of this study support the reaction being under thermodynamic control, where a linear free-energy relationship was identified between initial rate and the thermodynamics of the LLHT C-H bond cleavage event (Figure 10). This is consistent with the strength of the Ni-C bond strongly influencing reactivity and previous computational investigations that have shown that the Ni-C_{aryl} bond is formed early in the transition state.[6] The identification of thermodynamic control in these systems will potentially expedite catalyst design efforts that aim to increase the activity of nickel-mediated C-H bond activation.

The overall complexity of nickel-catalyzed hydroarylation via C-H functionalization reactions, including multiple competing reaction pathways, and the energetic parameters influencing reactivity and selectivity elucidated by this investigation are highlighted in Figure 11. The details elucidated by this investigation will help assist in the development and widespread use of nickel-catalysis for the functionalization of C-H bonds. Since the off-cycle activity described by this study stems from ancillary ligands on the nickel pre-catalyst, this work will help guide the development of future protocols for the general application of nickel-catalysis for organic synthesis.

AUTHOR INFORMATION

Corresponding Authors

*jmontg@umich.edu
*paulzim@umich.edu

Notes

The authors declare no competing financial interest.

ASSOCIATED CONTENT

Supporting Information

Experimental and computational details. The Supporting Information is available free of charge on the ACS Publications website.

ACKNOWLEDGMENTS

A.J.N. and J.M. thank the NSF Center for Chemical Innovation: Center for Selective C–H Functionalization (CHE-1700982). P.M.Z. thanks the NSF for support through CHE-1551994. Professor Donna Blackmond (the Scripps Research Institute) Dr. Erik Plata (the Scripps Research Institute), and Professor Christo Sevov (Ohio State University) are thanked for helpful discussions.

REFERENCES

(1) Davies, H. M. L., Morton, D. *J. Org. Chem.*, **2016**, 81, 343–350.

(2) For reviews on first-row transition metal catalyzed C-H functionalization see: (a) Pierpont, A. W.; Cundari, T. R. *Inorg. Chem.*, **2010**, 49, 2038–2046. (b) Kulkarni, A. A.; Daugulis, O. *Synthesis* **2009**, 4087. (c) Castro, L. C. M.; Chatani, N. *Chem. Lett.*, **2015**, 44, 410–421. (d) Miao, J.; Ge, H. *Eur. J. Org. Chem.*, **2015,** 36, 7859–7868. (d) Sperger, T.; Italo A. S.; Indrek K.; Franziska S. *Chem. Rev*., **2015**, 115, 9532–9586. (e) Johnson, S. A.; Hatnean J. A.; Doster M. E. *Prog. Inorg. Chem*., **2012**, 57, 255–352.

(3) Nakao, Y. *The Chem. Record*, **2011**, 11, 242–251.

(4) Nett, A. J., Zhao, W., Zimmerman, P. M., Montgomery, J. *J. Am. Chem. Soc.* **2015**, 137, 7636–7639.

(5) Xu, H.; Muto, K.; Yamaguchi, J.; Zhao, C.; Itami, K.; Musaev, D. G. *J. Am. Chem. Soc.* **2014**, 136, 14834–14844.

(6) Guihaumé, J.; Halbert, S.; Eisenstein, O; Perutz, R. N. *Organometallics* **2012**, 31, 1300–1314.

(7) For mechanistic investigation of nickel-catalyzed C-H functionalization see: (a) Johnson, S. A.; Doster, M. E., Matthews, J.; Shoshani, M.; Thibodeau, M.; Labadie, A.; Hatnean, J. A. *Dalton Trans.* **2012**, 41, 8135. (b) Xiao, L.-J.; Fu, X.-N.; Zhou, M.-J.; Xie J.-H.; Wang, L.-X.; Xu, X.-F.; Zhou, Q.-L. *J. Am. Chem. Soc.* **2016**, 138, 2957–2960. (c) Jiang, Y.-Y.; Li, Z.; Shi, J. *Organometallics* **2012**, 31, 4356–4366. (d) Kanyiva, K. S.; Kashihara, N.; Nakao, Y.; Hiyama, T.; Ohashi, M.; Ogoshi, S. *Dalton Trans.* **2010**, 39, 10483-10494. (e) Singh, V.; Nakao, Y.; Sakaki, S.; Deshmukh, M. M. *J. Org. Chem.*, **2017**, 82, 289–301. (f) Jiang, Y.-Y.; Li, Z.; Shi, J. *Organometallics*, **2012**, 31, 4356–4366. (g) Johnson, S. A. *Dalton Trans.*, **2015**, 44, 10905–10913.

(8) Schramm, Y.; Takeuchi, M.; Semba, K.; Nakao, Y.; Hartwig, J. F. *J. Am. Chem. Soc.*, **2015**, 137, 12215–12218.

(9) Bair, J. S.; Schramm, Y.; Sergeev, A. G.; Clot, E.; Eisenstein, O.; Hartwig, J. F. *J. Am. Chem. Soc.*, **2014**, 136, 13098-13101.

(10) (a) Watson, M. P.; Jacobsen, E. N. *J. Am. Chem. Soc.* **2008**, 130, 12594-12595. (b) Standley, E. A.; Jamison, T. F. *J. Am. Chem. Soc.* **2013**, 135, 1585-1592. (c) Staudaher, N. D.; Stolley, R. M.; Louie, J. *Chem. Commun.* **2014**, 50, 15577-15580. (d) Cornella, J.; Gomez-Bengoa, E.; Martin, R.́ *J. Am. Chem. Soc.* **2013**, 135, 1997-2009. (e) Shields, J. D.; Ahneman, D. T.; Graham, T. J. A.; Doyle, A. G. *Org. Lett.* **2014**, 16, 142-145.

(11) Montgomery, J. Organonickel Chemistry. In *Organometallics in Synthesis: Fourth Manual*; Lipshutz, B. H., Ed.; Wiley: Hoboken, NJ, **2013**; pp 319– 428.

(12) Nyce, G. W.; Csihony, S.; Waymouth, R. M.; Hedrick, J. L. *Chem. Eur. J.* **2004**, 10, 4073-4079.

(13) Mechanistic studies on palladium-mediated chain walking: (a) Hilton, M. J., Xu, L.-P., Norrby, P.-O., Wu, Y.-D., Wiest, O., Sigman, M. S. *J. Org. Chem.*, **2014**, 79, 11841–11850. (b) Shultz, L. H.; Brookhart, M. *Organometallics*, **2001**, 20, 3975–3982.

(14) (a) Juliá-Hernández, F.; Moragas, T.; Cornella, J.; Martin, R. *Nature*, **2017**, 545, 84–88. (b) Pappas, I.; Treacy, S.; Chirik, P. J. *ACS Catalysis*, **2016**, 6, 4105–4109. (c) Hicks, F. A.; Jenkins, J. C.; Brookhart, M. *Organometallics*, **2003**, 22, 3533-3545. (d) Mei, T. S.; Patel, H. H.; Sigman, M. S. *Nature,* **2014**, 508, 340-344.

(15) Experimental investigations of cationic nickel β-agostic interactions: (a) Xu, H., White, P. B., Hu, C., Diao, T. *Angew. Chem. Int. Ed.*, **2017**, 56, 1535–1538. (b) Svejda, S. A.; Johnson, L. K.; Brookhart, M. *J. Am. Chem. Soc.*, **1999**, 121, 10634–10635. (c) Leatherman, M. D.; Svejda, S. A.; Johnson, L. K.; Brookhart, M. *J. Am. Chem. Soc.*, **2003**, 125, 3068–3081.

(16) Computational studies on nickel β-agostic interactions: (a) Musaev, D. G.; Froese, R. D. J.; Svensson, M.; Morokuma, K. *J. Am. Chem. Soc.*, **1997**, 119, 367–374. (b) Deng, L.; Margl, P.; Ziegler, T *J. Am. Chem. Soc.*, **1997**, 119, 1094–1100.

(17) Blackmond, D. G. *Angew. Chem. Int. Ed.*, **2005**, 44, 4302–4320.

(18) Baxter, R. D.; Sale, D.; Engle, K. M.; Yu, J.-Q.; Blackmond, D. G. *J. Am. Chem. Soc.*, **2012**, 134, 4600–4606.

(19) (a) Burés, J. *Angew. Chem. Int. Ed.*, **2016**, 55, 2028–2031. (b) Burés, J. *Angew. Chem. Int. Ed.*, **2016**, 55, 16084–16087.

(20) Rodrigo, S. K.; Guan, H. *J. Org. Chem.*, **2017**, 82, 5230–5235.

(21) Sigman, M. S.; Harper, K. C.; Bess, E. N.; Milo, A. *Acc. Chem. Res.*, **2016**, 49, 1292–1301.

(22) For examples of BDE correlations see: (a) Jones, W. D.; Hessell, E. T. *J. Am. Chem. Soc.* **1993**, 115, 554–562. (b) Wick, D. D.; Jones, W. D. *Organometallics* **1999**, 18, 495–505. (c) Bryndza, H. E.; Fong, L. K.; Paciello, R. A.; Tam, W.; Bercaw, J. E. *J. Am. Chem. Soc.* **1987** 109, 1444–1456. (d) Clot, E.; Besora, M.; Maseras, F.; Mégret, C.; Eisenstein, O.; Oelckers, B., Perutz, R. N. *Chem. Comm.,* **2003**, 4, 490–491. (e) Clot, E.; Mégret, C.; Eisenstein, O.; Perutz, R. N. *J. Am. Chem. Soc.* **2009**, 131, 7817–7827. (f) Schaller, C. P.; Cummins, C. C.; Wolczanski, P. T. *J. Am. Chem. Soc.* **1996**, 118, 591–611.

(23) (a) Zimmerman, P. M. *J. Chem. Phys.* **2013**, 138, 184102. (b) Zimmerman, P. M. J. *Chem. Theory Comput.* **2013**, 9, 3043-3050. (c) Zimmerman, P. M. J. *Comput. Chem.* **2015**, 36, 601-611.

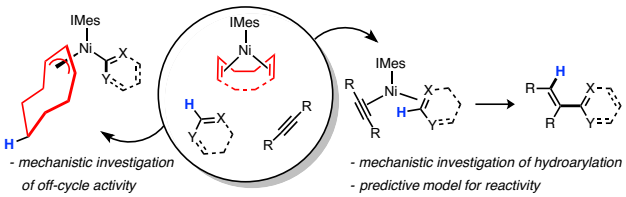

- *mechanistic investigation of off-cycle activity*

- *mechanistic investigation of hydroarylation*
- *predictive model for reactivity*